

**Locally resolved large scale phase separation in  
polymer:fullerene blends**

Journal:	<i>Journal of Materials Chemistry A</i>
Manuscript ID	TA-ART-09-2015-007004.R1
Article Type:	Paper
Date Submitted by the Author:	04-Nov-2015
Complete List of Authors:	Kästner, Christian; Technische Universität Ilmenau, Institute of Physics; Technische Universität Ilmenau, Institute of Thermodynamics and Fluid Mechanics Seeland, Marco; Technische Universität Ilmenau, Institute of Physics; Technische Universität Ilmenau, Institute of Computer and Systems Engineering Egbe, Daniel; Johannes Kepler University Linz, Linz Institute for Organic Solar Cells (LIOS) Hoppe, Harald; Technische Universität Ilmenau, Institute of Physics; Friedrich Schiller University Jena, Center for Energy and Environmental Chemistry Jena (CEEC Jena); Friedrich Schiller University Jena, Laboratory of Organic and Macromolecular Chemistry (IOMC)

# Locally resolved large scale phase separation in polymer:fullerene blends

Christian Kästner<sup>†a</sup>, Marco Seeland<sup>‡a</sup>, Daniel A.M. Egbe<sup>b</sup>, Harald Hoppe<sup>\*§Sa</sup>

*a* Institute of Physics, Technische Universität Ilmenau, Weimarer Str. 32, 98693 Ilmenau, Germany  
*b* Linz Institute for Organic Solar Cells, Johannes Kepler University, Altenbergerstr. 69, 4040 Linz, Austria

Current addresses:

<sup>†</sup> Institute of Thermodynamics and Fluid Mechanics, Technische Universität Ilmenau, Helmholtzring 1, 98693 Ilmenau, Germany

<sup>‡</sup> Institute of Computer and Systems Engineering, Technische Universität Ilmenau, Helmholtzplatz 5, 98693 Ilmenau, Germany

<sup>§</sup> Center for Energy and Environmental Chemistry Jena (CEEC Jena), Friedrich Schiller University Jena, Philosophenweg 7a, 07743 Jena, Germany

<sup>S</sup> Laboratory of Organic and Macromolecular Chemistry (IOMC), Friedrich Schiller University Jena, Humboldtstrasse 10, 07743 Jena, Germany

\* Corresponding author; Email: [Harald.Hoppe@uni-jena.de](mailto:Harald.Hoppe@uni-jena.de)

**Abstract:** We report a comprehensive study probing the influence of polymer blending on the large scale phase separation by use of electroluminescence imaging (ELI) and light-beam induced current (LBIC) measurements. The study is based on a semi-crystalline and an amorphous analogue of anthracene-containing poly(*p*-phenylene-ethynylene)-*alt*-poly(*p*-phenylene-vinylene) (PPE-PPV) copolymer (AnE-PVs) blended with [6,6]-phenyl-C61-butyric acid methyl ester (PCBM). Since the semi-crystalline polymer AnE-PV*ab* strongly phase separates from PCBM, whereas the amorphous polymer AnE-PV*ba* intimately mixes with PCBM, the phase separation is precisely controlled by blending both polymers in distinct ratios. The analysis of electroluminescence images and light-beam induced current scans allowed to conclude about domain size of phase separated bulk material and intermixed regions respectively, with the advantage of probing the whole active layer of the device at once.

## Introduction

The morphology of bulk heterojunction (BHJ) photoactive layers is supposed to crucially influence the device efficiency of polymer based organic photovoltaics (OPV).<sup>1,2,3,4</sup> Since the development of the BHJ concept<sup>5,6,7</sup> the power conversion efficiencies of polymer solar cells steadily increased, lately exceeding 10%.<sup>8,9,10</sup> This increase is not only originating from the consequent materials development of new high performing donor polymers and acceptor fullerene derivatives but also due to precise control of morphology in terms of phase separation between donor (D) and acceptor (A) as well as the interface between both.<sup>9,11,12,13,14,15</sup> Even though progress has been made concerning alternative acceptor materials<sup>16,17,18,19</sup> PCBM is still the most universal and commonly used fullerene derivative. Furthermore, it is common knowledge that the intermixed phase of polymer and PCBM yields high exciton dissociation rates and the phase separated pristine and primarily crystalline phases of polymer and PCBM support the charge transport of free holes and electrons by formation of an interpenetrating network.<sup>20,21,22</sup> This three phase system of an amorphous intimately mixed polymer:PCBM phase, locally separating the pristine crystalline polymer and a pristine crystalline PCBM phase, is crucial for the design of highly efficient OPV by preventing recombination of free charges across the heterojunction due to energetic relaxation.<sup>23,24,25</sup> Hence the energetic differences between energy levels of the highest

occupied molecular orbitals (HOMO) and the lowest unoccupied molecular orbitals (LUMO) in crystalline and amorphous polymers and acceptors facilitates the charge separation process.<sup>26,27,15</sup> Usually, the bulk morphology is quantitatively probed by x-ray scattering techniques, e.g. grazing incidence wide angle x-ray scattering (GiWAXS) for investigating the crystallinity and orientation of crystals and resonant soft x-ray scattering (R-SoXS) for measuring interface roughness, domain size and purity<sup>28,29,30,31,9</sup>, whilst atomic force microscopy (AFM) is commonly used to probe the surface morphology which may also propagate into the bulk.<sup>32,33,34</sup> Unfortunately, such techniques are only suitable for investigating the phase separation on a nanoscale of comparably small areas. Furthermore, steady-state optical spectroscopy, such as absorption and photoluminescence, qualitatively provide insight into polymer order and domain size and offers the opportunity to average over large areas, but lacks local resolution.<sup>35,36,37,38,39</sup> To observe morphological changes or differences on large scale areas, optical microscopy<sup>40</sup> or photography can be used, but there is in general no detailed information about material properties available. Since the electronic properties – generation, recombination and current extraction – of the active layer are directly linked to the morphology, it is conceivable to use spatially resolving optoelectronic measurement techniques to allusively resolve the morphology. By quantitative evaluation of such measurements, it is possible to extract the local electronic properties, such as dark saturation current and series resistance of the active layer.<sup>41,42</sup> To investigate large scale variations in morphology on large area devices, imaging techniques like electroluminescence imaging (ELI) and scanning techniques like light-beam induced current (LBIC) measurements can be applied. Several studies report about investigating the morphology and phase separation by high-resolution imaging methods.<sup>43,44,45,46,47</sup> Commonly such techniques are used in order to investigate and discuss a small sized sample region of interest on the device. In the present study we report about large scale phase separation and investigate the whole sample. A large phase separation is generally containing concentration gradients between the pristine phases and can be resolved by imaging and scanning techniques, allowing to deduce the requirements directed to highly efficient BHJ morphologies.

## Experimental

The herein investigated polymer solar cells were based on two anthracene-containing PPE-PPV (poly(p-phenylene-ethynylene)-*alt*-poly(p-phenylene-vinylene)) alternating copolymers: first copolymer substituted with linear octyloxy side-chains at the PPE-part and branched 2-ethylhexyloxy side-chains at the PPV-part (AnE-PVab) and second copolymer substituted with branched 2-ethylhexyloxy side-chains at the PPE-part and linear octyloxy side-chains at the PPV-part (AnE-PVba). AnE-PVab is characterized by a semi-crystalline and AnE-PVba by an amorphous morphology. Synthesis and material properties of those copolymers are described in a previous study.<sup>48</sup> Initial results, optoelectronic and optical data, of polymer:PCBM blends and polymer:polymer:PCBM blends and the corresponding preparation protocols are detailed in reference [49]. Furthermore, time-resolved spectroscopy<sup>50,51</sup> and structural properties<sup>52</sup> were carried out as well.

LBIC scans were conducted with a home-built setup using a Keithley 2400 source measure unit to extract the local short-circuit currents on a resolution of 100  $\mu\text{m}$ . The laser excitation wavelength used was 445 nm in order to excite both the polymer and the PCBM. To selectively excite the polymer additional scans at 532 nm were carried out. By comparing both measurements, obtained at 445 nm and 532 nm, the contribution of polymer and PCBM to the extracted short-circuit currents could be estimated and the phase separation was determined.

ELI measurements were performed with a cooled silicon charge-coupled-device (Si-CCD) camera with enhanced NIR sensitivity as described before.<sup>53,54</sup> To verify the phase separation,

ELI measurements with spectral selection of pristine donor and D/A-interface emission were performed by using a long-pass filter with a cut-off wavelength of 840 nm. All ELI measurements were background corrected by subtraction of corresponding measurements without excitation. For more details on the calculation of phase separation, see reference [42]. Electroluminescence spectra were recorded with an Avantes AvaSpec ULS-2048 fiber spectrometer in a home-built setup. A Keithley 2601 Source Measure Unit was used for excitation of the samples with a 100 mA injection current under forward bias. Photographs were taken with an ordinary digital camera Panasonic Lumix DMC-FZ3.

## Results

At first glance we characterized the spatial phase separation by photography, shown in Fig. 1. Obviously, the phase separation took place on a remarkably large extent and is directly determined by the blending ratio of semi-crystalline AnE-PVab and amorphous AnE-PVba.

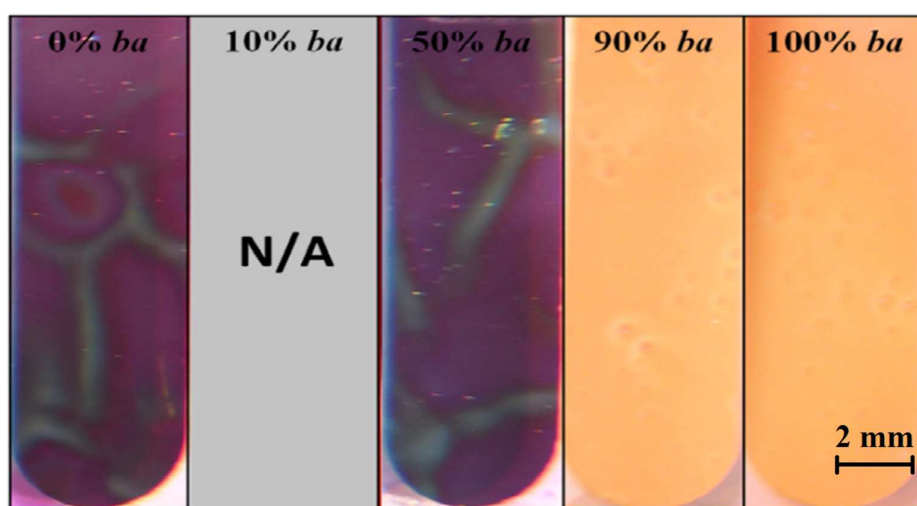


**Fig. 1** Photographs of solar cell active layers for various AnE-PVab:AnE-PVba:PCBM blends. The bright spots are due to residual dust on the samples.

In binary AnE-PVab:PCBM blends phase separation occurred to a large extent, but domains became smaller and evenly distributed upon addition of 10% AnE-PVba. The bright trenches within the active layers originate from the aluminium back contact due to large local film thickness variation. The active layers seemed to form islands by local dewetting of the active layer from the substrate during fabrication. In contrast, 90% and larger concentrations of AnE-PVba led to apparently homogeneous films.

To gain deeper insight into local phase separation, which might be non-detectable by photography, and its influence on local optoelectronic properties, LBIC and ELI measurements were conducted. Fig. 4 ELI pictures of solar cells fabricated from various AnE-PVab:AnE-PVba:PCBM ternary blends. The left hand side shows ELI measurements without spectral selection while on the right hand the calculated relative polymer emission is shown.

Of further importance is the size of polymer domains, which controls charge generation and hole transport.<sup>50,52</sup> If the polymer domain size exceeds the exciton diffusion length, the charge generation process is locally impeded under illumination whilst only monopolar hole

transport may occur under forward injection. If the polymer domains are small enough for allowing exciton diffusion to an adjacent D/A interface, and at the same time large enough for sufficient hole transport, the maximum photocurrent is expected from that favourable morphology. To elucidate the impact of local pristine polymer phase enrichment on charge generation and extraction,

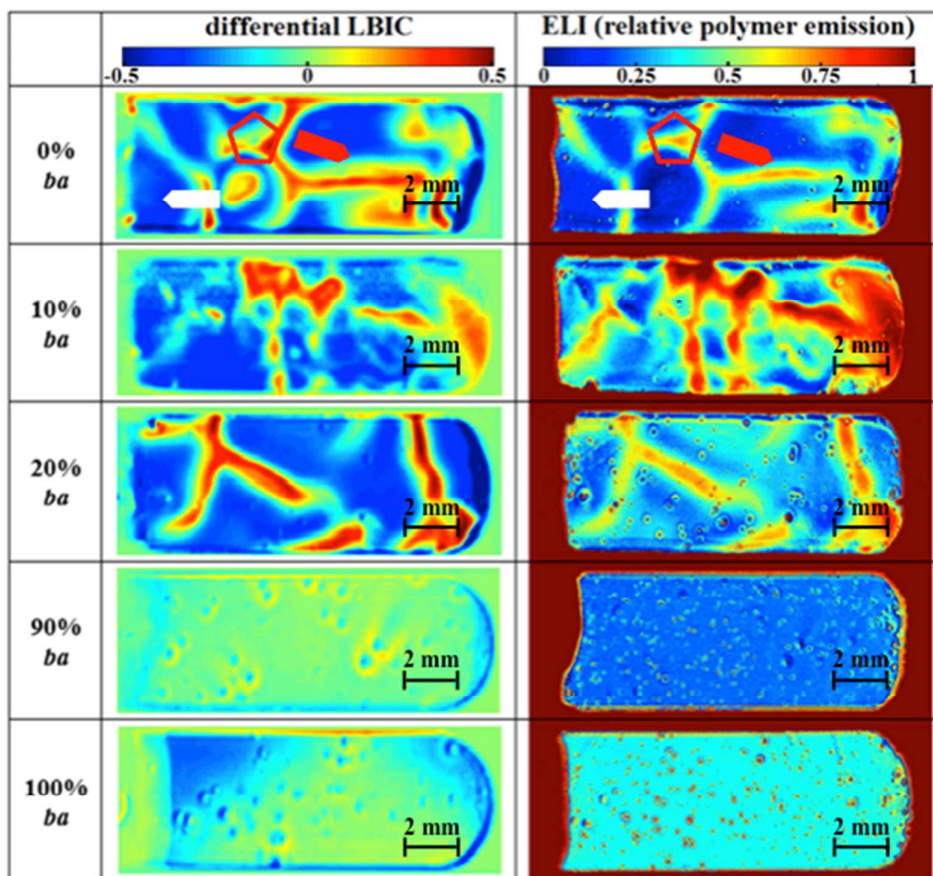
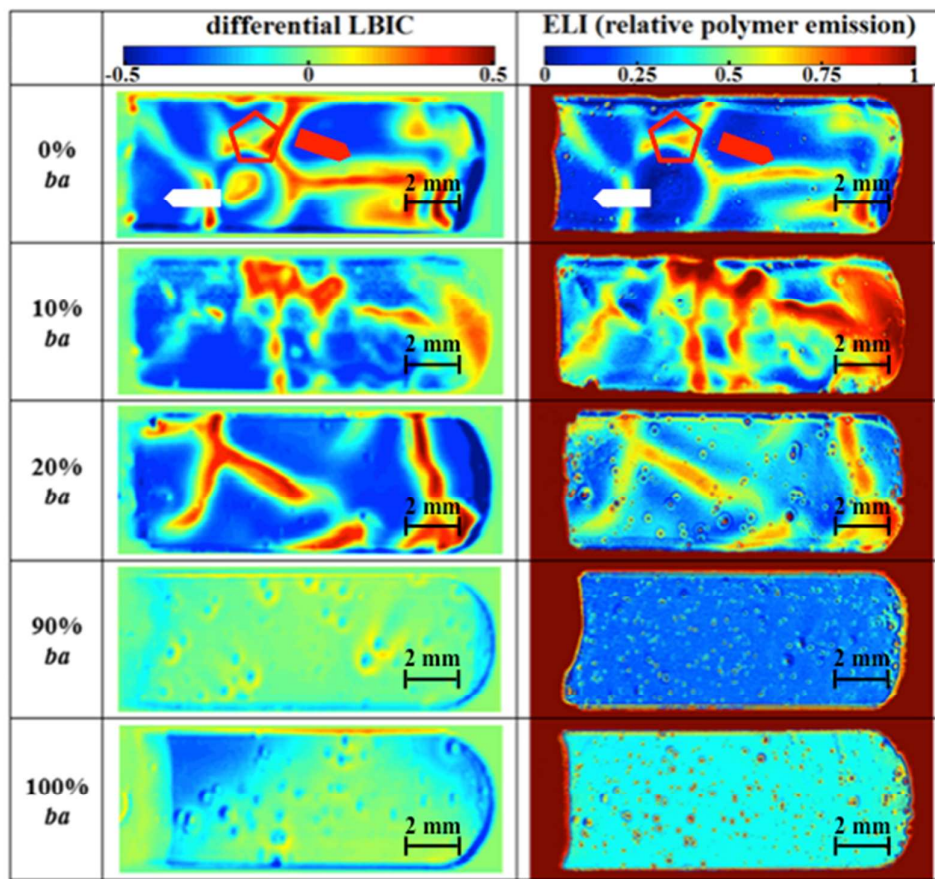
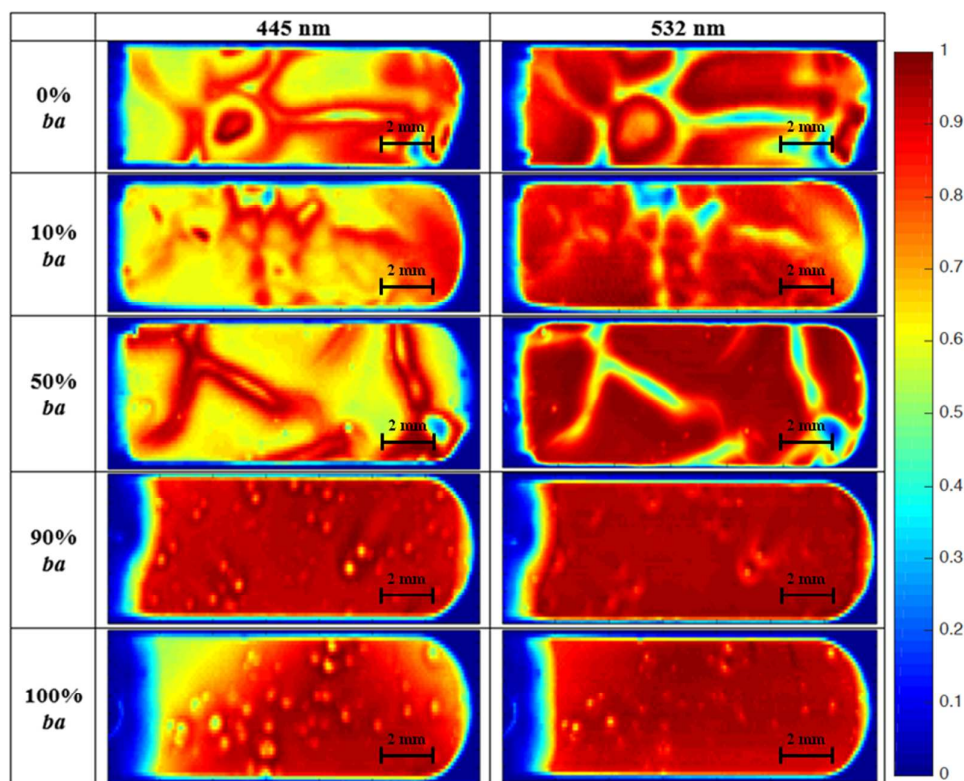


Fig. 5 depicts differential polymer maps by  $(\text{LBIC}_{532} - \text{LBIC}_{445}) / \text{LBIC}_{532}$  in comparison to the corresponding polymer emission obtained from ELI. Whereas ELI displays all percolating polymer phases, independent of their domain size, the differential LBIC displays the polymer domain size dependent charge collection as sum of charge generation and transport. Hence the comparison between LBIC and ELI allows to roughly estimate polymer domain sizes: either they support generation and percolation or percolation only. The differential LBIC shown in Fig. 5 mostly coincides with the ELI, but local variations can be observed. Taking a closer look further reveals that several intense structures observed in differential LBIC are parallel-translated against the structures detected by ELI (red markers in Figure 5). Hence they might be at the edges of pristine polymer domains. The blue rim for the 90% and 100% *ba* results from slightly mismatched position of the sample between the samples and is only visible as the differential signal is almost zero (compare with Figure 2).



**Fig. 5** Comparison of differential LBIC map and corresponding ELI data, emphasizing the location of pristine polymer domains. The red pentagon and arrow exemplarily display parallel-translated structures whereas the white arrow points on an exemplary homogeneous area.

depicts LBIC scans of fabricated solar cells for two different excitation wavelengths, 445 nm for the dominant absorption of PCBM and 532 nm for the dominant absorption of AnE-PV. The scans for 0%, 10% and 50% AnE-PV*ba* show clearly visible differences for the two different excitation wavelengths and manifest the strong phase separation. Hence the two different excitations mostly led to complementary successful photocurrent generation. For 90% and 100% AnE-PV*ba* no inhomogeneity from phase separation is detected. Only spots of lower photocurrent are observed at mutually coinciding positions, thus they were likely caused by local degradation or processing defects.<sup>53</sup>



**Fig. 2** Full-size LBIC scans of solar cells fabricated from various AnE-PVab:AnE-PVba:PCBM blends. Scans were taken for two different excitation wavelengths to primarily excite the PCBM at 445 nm and the polymers at 532 nm. Short-circuit currents were normalized to the respective maximal value: 0% *ba*: 2.0  $\mu\text{A}$  @ 445 nm (1  $\mu\text{A}$  @ 532 nm), 10% *ba*: 1.3  $\mu\text{A}$  (1.5  $\mu\text{A}$ ), 50% *ba*: 2.6  $\mu\text{A}$  (0.9  $\mu\text{A}$ ), 90% *ba*: 2.6  $\mu\text{A}$  (3  $\mu\text{A}$ ), 100% *ba*: 2.2  $\mu\text{A}$  (2.5  $\mu\text{A}$ ).

In Fig. 3 the electroluminescence spectra of the various blends investigated are depicted. The spectra can be generally divided into emissions arising from pristine – and potentially large scale phase separated – polymer domains in the range between 580-750 nm, and those emissions arising from charge transfer (CT) excitons originating from the intimately intermixed phase in the range between 750-1150 nm.<sup>49,50</sup> Employing the spectrally resolved information within the electroluminescence imaging setup by use of long-pass cut-off filters, phase separation can be readily detected as shown in Fig. 4. Whereas increased EL emission of the polymer phase was observed for zero and moderate *ba*-concentrations, no such phase separation was observed for 90% and 100% of AnE-PVba. Furthermore the contrast due to phase separation became less pronounced upon increasing *ba*-concentration.

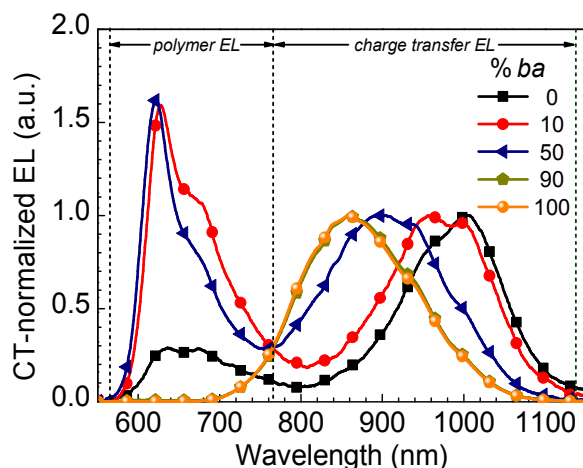


**Fig. 3** CT-normalized EL spectra of solar cells fabricated from various AnE-PVab:AnE-PVba:PCBM blends.

By spectral selection of the EL signal with a long-pass filter the relative increase of the emission of the polymer phase was calculated.<sup>42</sup> The corresponding images are depicted in Fig. 4 in the right column. The shorter wavelength EL emission strongly depends on the local AnE-PVba concentration. The trenches observed by photography and LBIC were resolved by ELI as well.

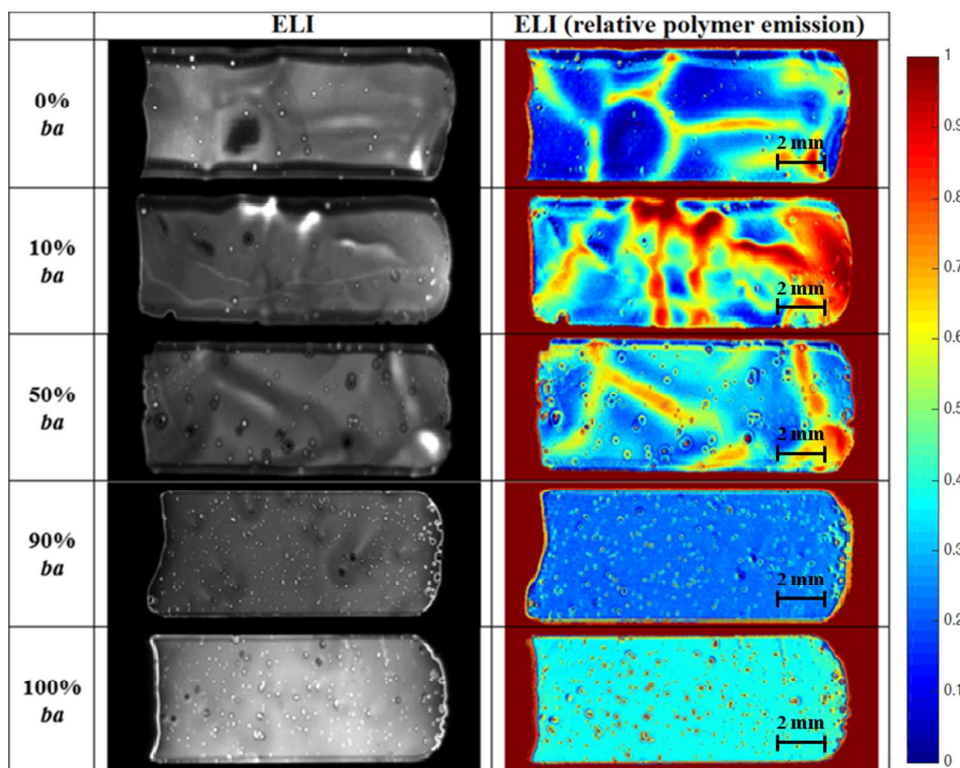


**Fig. 4** ELI pictures of solar cells fabricated from various AnE-PVab:AnE-PVba:PCBM ternary blends. The left hand side shows ELI measurements without spectral selection while on the right hand the calculated relative polymer emission is shown.

Of further importance is the size of polymer domains, which controls charge generation and hole transport.<sup>50,52</sup> If the polymer domain size exceeds the exciton diffusion length, the

charge generation process is locally impeded under illumination whilst only monopolar hole transport may occur under forward injection. If the polymer domains are small enough for allowing exciton diffusion to an adjacent D/A interface, and at the same time large enough for sufficient hole transport, the maximum photocurrent is expected from that favourable morphology. To elucidate the impact of local pristine polymer phase enrichment on charge extraction,

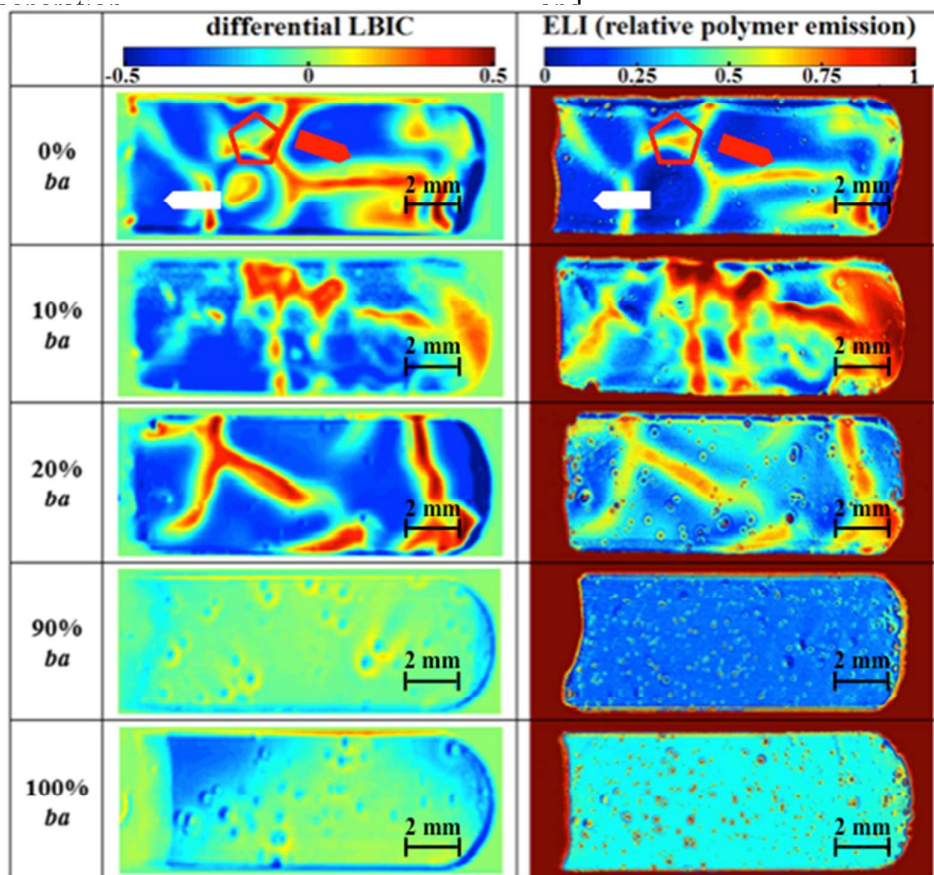
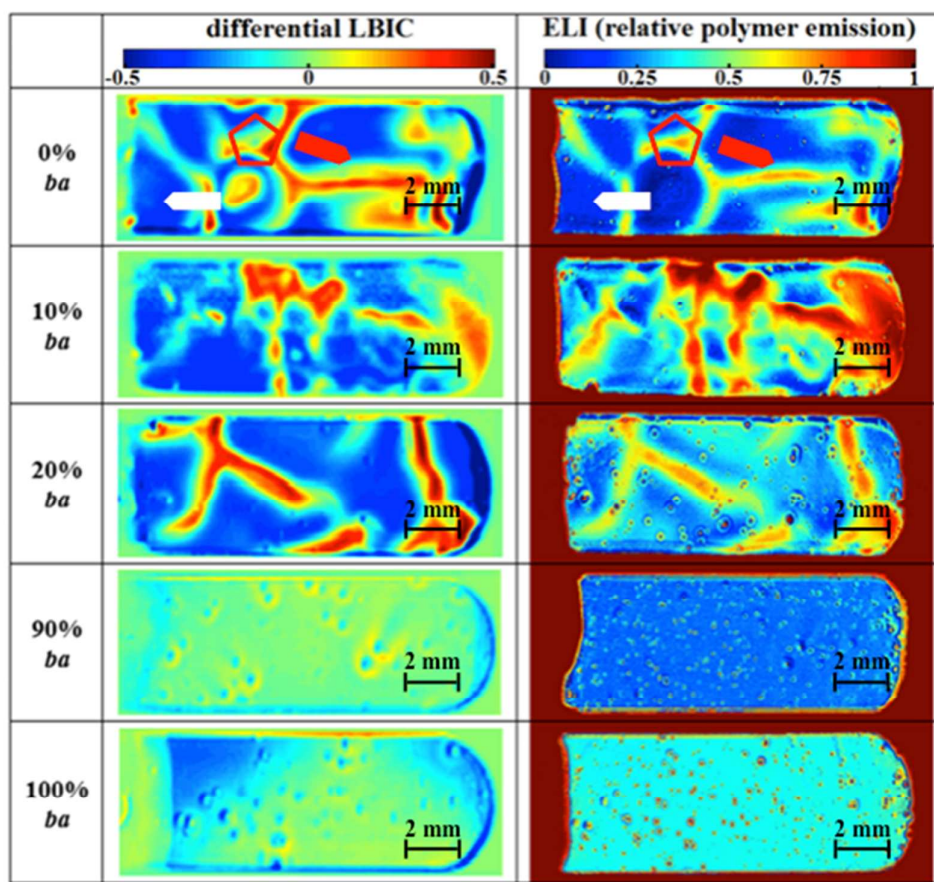


Fig. 5 depicts differential polymer maps by  $(\text{LBIC}_{532} - \text{LBIC}_{445}) / \text{LBIC}_{532}$  in comparison to the corresponding polymer emission obtained from ELI. Whereas ELI displays all percolating polymer phases, independent of their domain size, the differential LBIC displays the polymer domain size dependent charge collection as sum of charge generation and transport. Hence the comparison between LBIC and ELI allows to roughly estimate polymer domain sizes: either they support generation and percolation or percolation only. The differential LBIC shown in Fig. 5 mostly coincides with the ELI, but local variations can be observed. Taking a closer look further reveals that several intense structures observed in differential LBIC are parallel-translated against the structures detected by ELI (red markers in Figure 5). Hence they might be at the edges of pristine polymer domains. The blue rim for the 90% and 100% *ba* results from slightly mismatched position of the sample between the samples and is only visible as the differential signal is almost zero (compare with Figure 2).



**Fig. 5** Comparison of differential LBIC map and corresponding ELI data, emphasizing the location of pristine polymer domains. The red pentagon and arrow exemplarily display parallel-translated structures whereas the white arrow points on an exemplary homogeneous area.

## Discussion

Since charge generation takes place at the polymer:PCBM interface, LBIC maps the local mixing/demixing of polymer and PCBM or the local size of interfacial area, respectively. Regions generating low photocurrent for both polymer and PCBM dominant excitation (532 nm and 445 nm) reflect the single material enriched phases, but also bulk depleted regions of locally very thin active layer. In the present case the regions with low generation for both excitations fit to the trenches observed by photography. Comparing both LBIC measurements (445 nm and 532 nm) the photocurrent generation is similarly large at the rim of trenches (green colour in Figure 5), pointing towards an optimal phase separation to dominantly generated excitons in both materials, AnE-PV and PCBM, which then split at the interface. Comparing the emission spectra shown in Fig. 3 it is conclusive that the relatively increased emission extracted from spectrally selective ELI dominantly originates from polymer emission as PCBM emission (at around 720 nm) is substantially low and only shows very small shoulder peaks for 0%, 10% and 50% AnE-PV*ba*. Interestingly, the polymer emission maps follow the trenches as observed by LBIC and photography, but do not exactly fit. Furthermore, the emission is weak inside the trenches, but large at the rim of trenches. The relation between pristine polymer phase and charge generation/extraction becomes conclusive if comparing the differential polymer map of  $(LBIC_{532} - LBIC_{445})/LBIC_{532}$  and the corresponding ELI. Only polymer phases with proper domain size and dispersion, not

exceeding the exciton diffusion length and facilitating the necessary interfacial area for splitting the excitons, contribute to the maximum charge generation as well as charge percolation. These regions appear dominant for both differential LBIC and ELI. The regions with large EL emission and reduced charge generation point onto large polymer domains, where excitons cannot reach the interface. Hence percolation is improved, but free charge generation is impeded due to reduced interfacial area. The spatial ratio of sufficiently percolating polymer phase to homogeneously intermixed phase gradually changes with concentration of AnE-PVba. This is not astonishing since the increase in amorphous polymer fraction reduces the phase separation ability.<sup>49</sup> The PCBM becomes dissolved within the amorphous polymer and the crystalline polymer phase totally shrinks as its concentration decreases. Interestingly, the percolating polymer phase domain size evolves more “fine-meshed” upon addition of 10% amorphous AnE-PVba. Hence a more favoured phase separation is concluded, which provides both hole percolation and free charge generation.

### Conclusions

We demonstrated detection of large scaled phase separation in ternary polymer:polymer:PCBM blends. The combination of light-beam induced current measurement and electroluminescence imaging enables investigation of large scale phase separation and domain size evolution, which are not detectable with conventional structural analysis subject to area averaging. Spectrally selective measurements allowed to differentiate between pristine phases and intimately mixed phases of polymer and PCBM. Furthermore, the comparison of LBIC and ELI allowed to confine the percolating polymer phase from the charge generation supporting phase and thus visualizes the spatial distribution of pristine polymer domains.

### Acknowledgements

The authors are grateful for financial support within the frame of "AIMS in OPV" (contract nr. 03EK3502) funded by the Federal Ministry of Education and Research (BMBF), and the Deutsche Forschungsgemeinschaft (DFG) and the Austrian Science Fund (FWF) (contract nr. I1703-N20) in the framework of D.A.CH project “PhotogenOrder”. CK gratefully acknowledges funding by the Thüringer Landesgraduiertenschule für Photovoltaik (PhotoGrad). MS gratefully acknowledges funding within the scholarship program of the Deutsche Bundesstiftung Umwelt (DBU). We thank the Thuringian Ministry of Culture for financial support in the framework of FIPV II.

### References

1. E. Moons, *Journal of Physics-Condensed Matter*, 2002, **14**, 12235-12260.
2. H. Hoppe and N. S. Sariciftci, in *Photoresponsive Polymers II*, eds. S. R. Marder and K. S. Lee, 2008, vol. 214, pp. 1-86.
3. M. T. Dang, L. Hirsch, G. Wantz and J. D. Wuest, *Chemical Reviews*, 2013, **113**, 3734-3765.
4. H. Hoppe and N. S. Sariciftci, *Journal of Materials Chemistry*, 2006, **16**, 45-61.
5. N. S. Sariciftci, L. Smilowitz, A. J. Heeger and F. Wudl, *Science*, 1992, **258**, 1474-1476.
6. G. Yu, J. Gao, J. C. Hummelen, F. Wudl and A. J. Heeger, *Science*, 1995, **270**, 1789-1791.
7. J. J. M. Halls, C. A. Walsh, N. C. Greenham, E. A. Marseglia, R. H. Friend, S. C. Moratti and A. B. Holmes, *Nature*, 1995, **376**, 498-500.

8. M. A. Green, K. Emery, Y. Hishikawa, W. Warta and E. D. Dunlop, *Progress in Photovoltaics: Research and Applications*, 2015, **23**, 805-812.
9. Y. Liu, J. Zhao, Z. Li, C. Mu, W. Ma, H. Hu, K. Jiang, H. Lin, H. Ade and H. Yan, *Nat Commun*, 2014, **5**.
10. Z. He, B. Xiao, F. Liu, H. Wu, Y. Yang, S. Xiao, C. Wang, T. P. Russell and Y. Cao, *Nat Photon*, 2015, **9**, 174-179.
11. J. Nelson, *Materials Today*, 2011, **14**, 462-470.
12. C. J. Brabec, M. Heeney, I. McCulloch and J. Nelson, *Chemical Society Reviews*, 2011, **40**, 1185-1199.
13. H. X. Zhou, L. Q. Yang and W. You, *Macromolecules*, 2012, **45**, 607-632.
14. P. P. Khlyabich, B. Burkhart and B. C. Thompson, *J. Am. Chem. Soc.*, 2012, **134**, 9074-9077.
15. P. P. Khlyabich, B. Burkhart, A. E. Rudenko and B. C. Thompson, *Polymer*, 2013, **54**, 5267-5298.
16. N. Zhou, H. Lin, S. J. Lou, X. Yu, P. Guo, E. F. Manley, S. Loser, P. Hartnett, H. Huang, M. R. Wasielewski, L. X. Chen, R. P. H. Chang, A. Facchetti and T. J. Marks, *Advanced Energy Materials*, 2014, **4**, n/a-n/a.
17. P. Cheng, X. Zhao, W. Zhou, J. Hou, Y. Li and X. Zhan, *Organic Electronics*, 2014, **15**, 2270-2276.
18. C. Lee, H. Kang, W. Lee, T. Kim, K.-H. Kim, H. Y. Woo, C. Wang and B. J. Kim, *Advanced Materials*, 2015, **27**, 2466-2471.
19. Z. Tang, B. Liu, A. Melianas, J. Bergqvist, W. Tress, Q. Bao, D. Qian, O. Inganäs and F. Zhang, *Advanced Materials*, 2015, **27**, 1900-1907.
20. X. N. Yang, J. Loos, S. C. Veenstra, W. J. H. Verhees, M. M. Wienk, J. M. Kroon, M. A. J. Michels and R. A. J. Janssen, *Nano Letters*, 2005, **5**, 579-583.
21. S. S. van Bavel, E. Sourty, G. de With and J. Loos, *Nano Letters*, 2009, **9**, 507-513.
22. C.-K. Lee and C.-W. Pao, *The Journal of Physical Chemistry C*, 2012, **116**, 12455-12461.
23. F. C. Jamieson, E. B. Domingo, T. McCarthy-Ward, M. Heeney, N. Stingelin and J. R. Durrant, *Chemical Science*, 2012, **3**, 485-492.
24. S. Gelinas, A. Rao, A. Kumar, S. L. Smith, A. W. Chin, J. Clark, T. S. van der Poll, G. C. Bazan and R. H. Friend, *Science*, 2014, **343**, 512-516.
25. B. M. Savoie, A. Rao, A. A. Bakulin, S. Gelinas, B. Movaghar, R. H. Friend, T. J. Marks and M. A. Ratner, *J. Am. Chem. Soc.*, 2014, **136**, 2876-2884.
26. I. W. Hwang, D. Moses and A. J. Heeger, *Journal of Physical Chemistry C*, 2008, **112**, 4350-4354.
27. O. G. Reid, J. A. N. Malik, G. Latini, S. Dayal, N. Kopidakis, C. Silva, N. Stingelin and G. Rumbles, *Journal of Polymer Science Part B-Polymer Physics*, 2012, **50**, 27-37.
28. J. Perlich, J. Rubeck, S. Botta, R. Gehrke, S. V. Roth, M. A. Ruderer, S. M. Prams, M. Rawolle, Q. Zhong, V. Körstgens and P. Müller-Buschbaum, *Review of Scientific Instruments*, 2010, **81**, -.
29. S. Swaraj, C. Wang, H. Yan, B. Watts, J. Lüning, C. R. McNeill and H. Ade, *Nano Letters*, 2010, **10**, 2863-2869.
30. L. Ye, S. Zhang, W. Ma, B. Fan, X. Guo, Y. Huang, H. Ade and J. Hou, *Advanced Materials*, 2012, **24**, 6335-6341.
31. W. Ma, J. R. Tumbleston, M. Wang, E. Gann, F. Huang and H. Ade, *Advanced Energy Materials*, 2013, **3**, 864-872.
32. M. Kemerink, J. K. J. van Duren, P. Jonkheijm, W. F. Pasveer, P. M. Koenraad, R. A. J. Janssen, H. W. M. Salemink and J. H. Wolter, *Nano Letters*, 2003, **3**, 1191-1196.

33. C. Kastner, D. K. Susarova, R. Jadhav, C. Ulbricht, D. A. M. Egbe, S. Rathgeber, P. A. Troshin and H. Hoppe, *Journal of Materials Chemistry*, 2012, **22**, 15987-15997.
34. C. R. Singh, G. Gupta, R. Lohwasser, S. Engmann, J. Balko, M. Thelakkat, T. Thurn-Albrecht and H. Hoppe, *Journal of Polymer Science Part B-Polymer Physics*, 2013, **51**, 943-951.
35. R. Osterbacka, C. P. An, X. M. Jiang and Z. V. Vardeny, *Science*, 2000, **287**, 839-842.
36. K. Pichler, D. A. Halliday, D. D. C. Bradley, P. L. Burn, R. H. Friend and A. B. Holmes, *Journal of Physics-Condensed Matter*, 1993, **5**, 7155-7172.
37. J. Clark, J. F. Chang, F. C. Spano, R. H. Friend and C. Silva, *Applied Physics Letters*, 2009, **94**.
38. F. C. Spano, J. Clark, C. Silva and R. H. Friend, *Journal of Chemical Physics*, 2009, **130**.
39. M. Hallermann, I. Kriegel, E. Da Como, J. M. Berger, E. von Hauff and J. Feldmann, *Adv. Funct. Mater.*, 2009, **19**, 3662-3668.
40. V. Turkovic, S. Engmann, G. Gobsch and H. Hoppe, *Synthetic Metals*, 2012, **161**, 2534-2539.
41. M. Seeland, R. Rosch and H. Hoppe, *Journal of Applied Physics*, 2012, **111**.
42. M. Seeland, C. Kästner and H. Hoppe, *Applied Physics Letters*, 2015, **107**, 073302.
43. D. P. Ostrowski and D. A. Vanden Bout, *Small*, 2014, **10**, 1821-1829.
44. J. L. Luria, N. Hoepker, R. Bruce, A. R. Jacobs, C. Groves and J. A. Marohn, *ACS Nano*, 2012, **6**, 9392-9401.
45. X. T. Hao, L. M. Hirvonen and T. A. Smith, *Methods and Applications in Fluorescence*, 2013, **1**, 015004.
46. A. Perulli, S. Lattante, A. Persano, A. Cola, M. Di Giulio and M. Anni, *Applied Physics Letters*, 2013, **103**, 053305.
47. T. J. K. Brenner and C. R. McNeill, *The Journal of Physical Chemistry C*, 2011, **115**, 19364-19370.
48. D. A. M. Egbe, S. Türk, S. Rathgeber, F. Kühnlenz, R. Jadhav, A. Wild, E. Birckner, G. Adam, A. Pivrikas, V. Cimrova, G. n. Knör, N. S. Sariciftci and H. Hoppe, *Macromolecules*, 2010, **43**, 1261-1269.
49. C. Kästner, S. Rathgeber, D. A. M. Egbe and H. Hoppe, *Journal of Materials Chemistry A*, 2013, **1**, 3961.
50. H. Mangold, A. A. Bakulin, I. A. Howard, C. Kastner, D. A. M. Egbe, H. Hoppe and F. Laquai, *Physical Chemistry Chemical Physics*, 2014.
51. M. T. Sajjad, A. J. Ward, C. Kästner, A. Ruseckas, H. Hoppe and I. D. W. Samuel, *The Journal of Physical Chemistry Letters*, 2015, 3054-3060.
52. C. Kästner, X. Jiao, D. A. M. Egbe, H. Ade and H. Hoppe, 2014.
53. M. Seeland, R. Rosch and H. Hoppe, *Journal of Applied Physics*, 2011, **109**.
54. M. Seeland, R. Rösch and H. Hoppe, in *Stability and Degradation of Organic and Polymer Solar Cells*, ed. F. C. Krebs, John Wiley & Sons, 2012.

## Locally resolved large scale phase separation in polymer:fullerene blends

Christian Kästner, Marco Seeland, Daniel A.M. Egbe, Harald Hoppe

Large scale phase separation in polymer:fullerene bulk heterojunction solar cells investigated by electroluminescence imaging (ELI) and light-beam induced current (LBIC) measurement.

